Vol 17 No 11, November 2008
1674-1056/2008/17(11)/4247-06

Chinese Physics B

© 2008 Chin. Phys. Soc.
and IOP Publishing Ltd

Single crystalline boron carbide nanobelts: synthesis and characterization*

Bao Li-Hong(鲍丽宏), Li Chen(李 晨), Tian Yuan(田 园), Tian Ji-Fa(田继发), Hui Chao(惠 超), Wang Xing-Jun(王兴军), Shen Cheng-Min(申承民), and Gao Hong-Jun(高鸿钧)†

National Laboratory for Condensed Matter Physics, Institute of Physics, Chinese Academy of Sciences, Beijing 100190, *China*

(Received 24 March 2008; revised manuscript received 21 April 2008)

This paper reports that the large-scale single crystalline boron carbide nanobelts have been fabricated through a simple carbothermal reduction method with $B/B_2O_3/C/Fe$ powder as precursors at 1100°C. Transmission electron microscopy and selected area electron diffraction characterizations show that the boron carbide nanobelt has a B_4C rhomb-centred hexagonal structure with good crystallization. Electron energy loss spectroscopy analysis indicates that the nanobelt contains only B and C, and the atomic ratio of B to C is close to 4:1. High resolution transmission electron microscopy results show that the preferential growth direction of the nanobelt is [101]. A possible growth mechanism is also discussed.

Keywords: carbothermal reduction, boron carbide, nanobelts, vapour-solid
PACC: 6146, 9260

1. Introduction

Boron carbide is an important lightweight refractory semiconducting material due to its unique properties and potentially widespread applications. It has low density ($2.5 g\cdot cm^{-3}$), high melting point ($> 2400°C$), high strength and Young's modulus, and high-temperature thermal properties.[1−3] It is the third hardest material coming after the diamond and cubic boron nitride, but with very high temperature stability. It has a high neutron capture-section.[4] It has wide applications especially under extreme conditions, such as ceramic armours, neutron absorbers in the nuclear industry, and a potential material for high-temperature energy conversion.[1−5]

In past years, much effort has been devoted to the synthesis of boron carbide nanostructures, including carbothermal reduction of boron oxides,[6−10] chemical vapour deposition (CVD) and plasma enhanced CVD (PECVD),[11−14] Carbon Nanotubes (CNT) template assisted growth,[14−17] a porous alumina temple technique,[18] electrostatic pinning[19] and thermal evaporation of B_4C powder.[20] Boron carbide nanowires, nanonecklaces, nanosprings,[11,12,17] aligned nanofibres, and encapsulates of boron carbide nanowires into BN or boron carbonitride nanotubes[16] have been prepared.

In this paper, we report synthesis of single crystalline boron carbide nanobelts via an improved simple carbothermal reduction method with $B/B_2O_3/C$ powder as precursor. Transmission electron microscopy (TEM) and selected area electron diffraction (SAED) characterizations show that the boron carbide nanobelt has a B_4C rhomb-centred hexagonal structure[21] with good crystallization. Electron energy loss spectroscopy (EELS) spectrum indicates that the nanobelt contains only B and C, and the B to C atomic ratio is close to 4:1. High resolution TEM (HRTEM) results show that the preferential growth direction of the nanobelt is [101]. A possible growth mechanism is also discussed.

2. Experimental

2.1. Preparation of Fe_3O_4 nanoparticles

In past years, we have successfully fabricated a few kinds of nanoparticles.[22−26] Fe_3O_4 nanoparticles have been successfully used as catalyst to fabricate boron nanocones.[27] Here we use Fe_3O_4 nanoparticles to catalyse the growth of boron carbide nanobelts.

*Project supported by the National 863 (Grant No 2007AA03Z305) and 973 (Grant No 2007CB935503) program, the National Science Foundation of China (Grant Nos 60571045, 60620120443, Guo-JI He-Zuo).
†Corresponding author. E-mail: hjgao@aphy.iphy.ac.cn

Fe_3O_4 nanoparticles with diameters of less than 10 nm were synthesized by high temperature solution phase reduction of iron (III) acetylacetonate, with 1,2-hexadecanediol in the presence of oleic acid and oleylamine.[28,29]

2.2. Fabrication of boron carbide nanobelts

The experiment was carried out in our home made tube furnace CVD system. The schema is shown in Fig.1. Ceramic boat at the inlet of the horizontal tube furnace was site A and site B is located at the centre of the furnace. All of the employed reactants were in analytical grade and were used without further purification. A mixture of boron powder (99.9%), B_2O_3 powder (99.99%), carbon powder (99.9%) and Fe powder (99.9%) with a weight ratio 2:2:1:1 was loaded into a ceramic boat after adequately milled. Several drops of Fe_3O_4 nanoparticles solution was firstly dropped onto a Si (111) wafer, and after the catalytic solution was dry the wafer was introduced into the ceramic boat keeping the surface of the wafer touched with the precursors. High purity argon gas (99.99%) was fed into the tube at a flow rate of 300 sccm for 0.5h prior to the temperature increasing processes during which the boat is kept at the site A (See Fig.1). A two-step procedure was performed to control the growth process. Firstly, the temperature at the furnace centre was increased to 250°C in 15 minutes, and then the ceramic boat was quickly transferred from site A to site B and held for half an hour to eliminate the remaining oleic acid and oleylamine of Fe_3O_4 nanoparticles. Then the boat was pulled from site B to site A. Secondly, the temperature was increased to 1100°C in 60 minutes. And once the temperature was arrived at 1100°C, the ceramic boat was quickly transferred from site A to site B again and held for 2h to grow the boron carbide nanobelts. The flow rate of the Ar gas was kept 300 sccm at the first step and then changed to 30 sccm at the second step. The environment pressure of the quartz tube was kept 1 atmospheric pressure. After the furnace was cooled down to room temperature, dark brown or black product was obtained on the surface of the substrate.

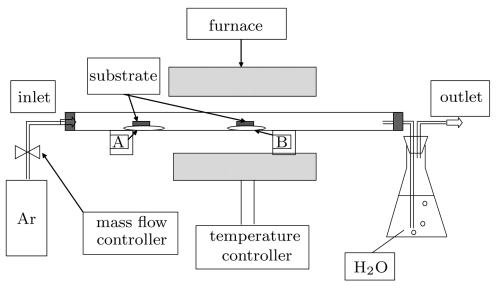


Fig.1. Schema of the CVD system for growth of boron carbide nanobelts.

2.3. Characterization of boron carbide nanowires

The morphologies of boron carbide nanobelts were observed by a field-emission type scanning electron microscope (SEM) (XL-SFEG, FEI Corp.). TEM (JEOL-200CX) and HRTEM (Tecnai F20, FEI Corp.) were used to further investigate the structure of the boron carbide belts. The chemical compositions of the boron carbide nanobelts were investigated by EELS. Linescan technique has been used to reveal the distribution of the elements in the boron carbide nanobelts.

3. Results and discussion

Figures 2(a)–2(f) are a series of SEM images of the as-synthesized nanobelts. Figure 2(a) is a low magnification SEM image, showing that large scale nanobelts have been successfully fabricated. A closer view reveals that the large scale nanobelts have a 'grass-like' morphology, shown in Fig.2(b). A higher magnification SEM image in Fig.2(c) indicates that these 'grass-like' nanobelts have a length of 10–20 μm. The high-resolution SEM (HRSEM) images in Figs.2(d)–2(f) reveal that the as-grown nanobelts have a width of 200–300 nm. From Figs.2(b) and 2(c), we can see that the nanobelts grow from common local sites and elongated at random directions like a cluster of grasses, and some nanobelts are typically twisted. In addition, the HRSEM images in Figs.2(d)–2(f) show that the nanobelts have uniform width.

Further structure characterization was performed by TEM and SAED. Figure 3(a) shows a low magnification TEM image several twisted nanobelts. The width of these nanobelts ranges from 200–300 nm, which is consistent with the results measured by SEM shown in Figs.2(d)–2(f). Electron diffraction was done

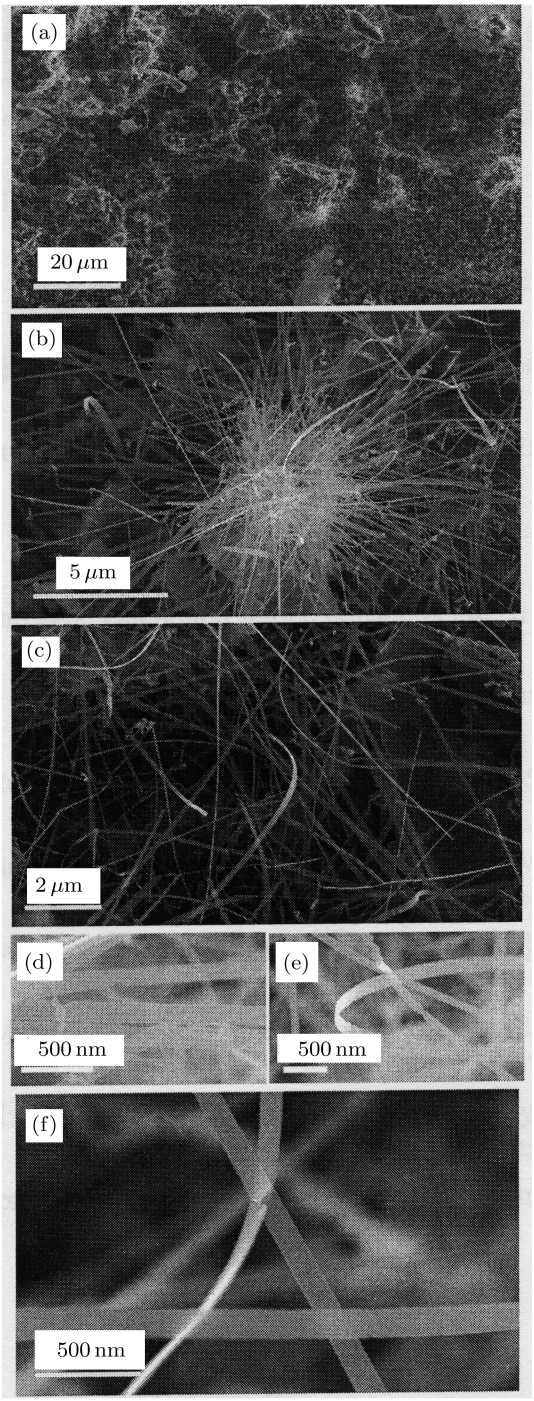


Fig.2. The SEM images of nanobelts. (a) The low-magnification SEM image of the large scale nanobelts. (b) 'Grass-like' nanobelts. (c) A higher magnification SEM image of this kind of nanobelts. (d)–(f) HRSEM images of different twisted nanobelts.

on several nanobelts to determine their structure. For each nanobelts, a series of diffraction patterns were recorded by titling the sample to different low-index zone axes. It was found that the nanobelts are crystalline. The calculated lattice constants are $a = 0.56 \pm 0.005$ nm and $c = 12.08 \pm 0.007$ nm, which coincide closely with the values of rhomb-centred hexagonal B_4C structure from the JCPDS database[21] (#35-0798: $a = 0.56$ nm, $c = 12.08$ nm). The inset in the Fig.3(a) is a representative diffraction patterns recorded from the thwartwise nanobelt in Fig.3(a) in [010] axis. Figure 3(b) is a representative HRTEM image, showing that the nanobelt is crystallized and covered by a 1–2nm thick amorphous layer, which is formed when the crystalline nanobelts was exposed to air. The preferential growth direction was determined to be the [101] direction.

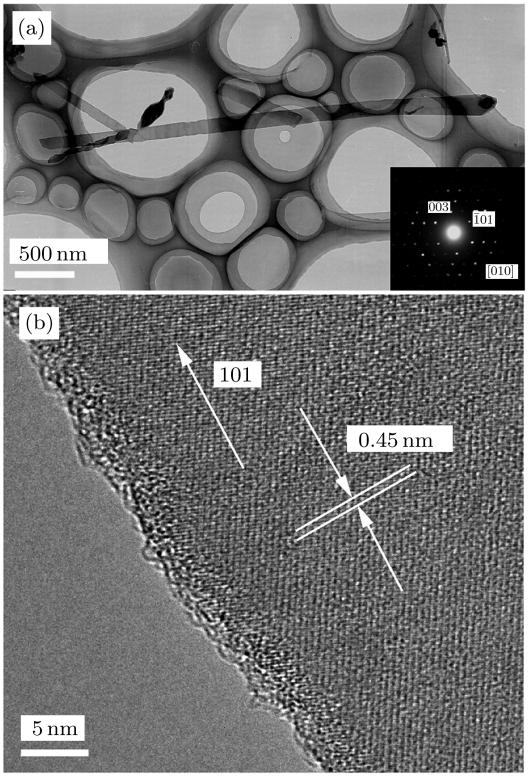


Fig.3. (a) TEM image of several twisted boron carbide nanobelts at low magnification. The inset is the SAED pattern recorded along [010] zone axis. (b) HRTEM image of part of the nanobelt, showing crystallized structure and the preferential growth along [101] zone. Note thin amorphous layer, left side.

Chemical compositions of the different parts of the nanobelts were analysed by EELS. Figure 4 depicts a typical EELS spectrum from the middle of the nanobelt. Ionization edges around 188 and 284 eV are observable in the spectrum corresponding to the K-ionization edges of boron and carbon, respectively. From Fig.4, no oxygen, iron or other impurities are detected, indicating that the nanobelt is only composed of B and C. Quantitative analysis of the EELS spectrum yields the elemental concentration of the

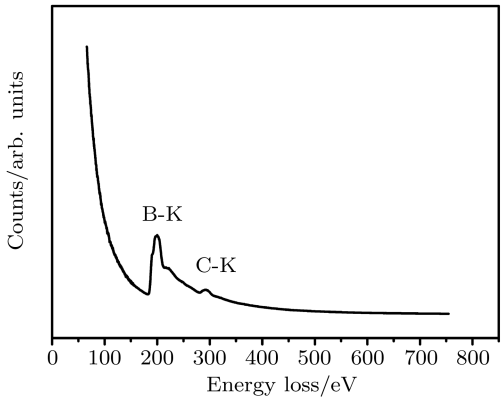


Fig.4. A representative EELS spectrum obtained from a boron carbide nanobelt, showing a boron core-loss peak at ~ 188 eV and a carbon core-loss peak at ~ 284 eV.

nanobelt. The atomic ratio of C to B is calculated as 0.26 ± 0.036, close to B_4C (C/B ~ 0.25).

To further analyse the chemical composition and the chemical structure of the nanobelts, cross-sectional energy dispersion spectroscopy (EDS) linescan was preformed, as is shown in Figs.5(a)–5(d). Figure 5(a) is the cross-sectional EDS linescan relative TEM image, the crossed grey line is the recorded site. The dark grey, grey and black curves in Figs.5(b)–5(d) correspond to the boron, carbon and oxygen element distribution in the nanobelt, respectively. From the detailed profiles shown in Fig.5(b)–5(d), we can see that boron and carbon are uniformly distributed in the nanobelt, while the concentration of oxygen is in trace degree. It further confirms that the as-grown nanobelts are crystalline B_4C nanobelts.

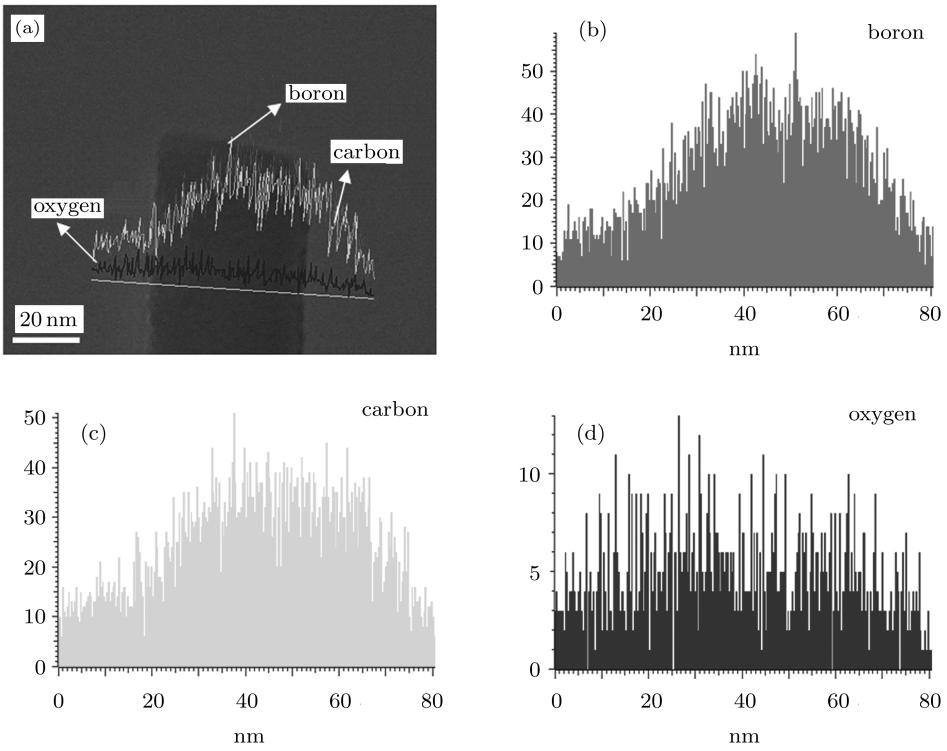


Fig.5. A typical EDS linescan profile of a boron carbide nanobelt. (a) A dark-field TEM image of a boron carbide nanobelt and relative elements distribution (B (dark grey curve), C (grey curve), O (black curve)). (b)–(d) is the detailed EDS linescan profiles for B (dark grey curve), C (grey curve) and O (black curve) respectively, recorded along the grey line indicated in Fig.5(a).

There are several growth mechanisms for nanostructures.[30] The widely-used vapour–liquid–solid (VLS) process[31] involves a liquid catalytic particle, typically located at the tip of the growing nanowire or nanotube. During the growth, the liquid phase catalytic droplets adsorb target atoms from the vapour phase source materials and nanowires or nanotubes precipitate from the droplets when the target materials in the droplets reach saturation. The VLS mechanism has ever been invoked to explain the growth of boron carbide nanowires.[7,11] Although Fe_3O_4 nanoparticles have been introduced to prepare the boron carbide nanobelts in here, no particles were observed at the end of the boron carbide nanobelts. Therefore the growth mechanism of the boron carbide nanobelts is not a VLS mechanism. Another mech-

anism for growth of semiconducting nanowires is the oxide-assisted-growth (OAG) mechanism,[32] in which an oxide layer formed on the outside of the nanowire is supposed to confine its lateral growth. The molten or near molten oxide layer might enhance atomic absorption, diffusion and deposition. As discussed above, although there is a thin amorphous oxide layer on the surface of the boron carbide nanobelts, we believe that the oxide layer was formed by oxidation after the nanobelts were exposed to ambience. The OAG mechanism is thus not relevant to the growth of these boron carbide nanobelts.

Vapour-solid (VS) growth mechanism has ever been adopted for the growth of boron carbide nanowires.[8] For the VS mechanism, surface energy, defects and vapour-related processes are often considered. In our case, Fe_3O_4 nanoparticles coated Si (111) wafer kept touching with the source powder materials in the ceramic boat during all the growth stages. The Fe_3O_4 nanoparticles on the Si surface may offer energy-preferred sites for the growth of nanobelts. We also attempted to synthesis boron carbide nanobelts without Fe_3O_4 catalytic particles, but no 1D boron carbide nanostructures were observed on the surface of the Si (111) wafer. Therefore the Fe_3O_4 nanoparticles play an important role in the growth of boron carbide nanobelts. In addition, at the high experimental temperature (1100°C), the following chemical reactions may take place:

$$B_2O_3(s) \xrightarrow{1100^\circ C} B_2O_3(g), \quad (1)$$

$$4B(s) + B_2O_3(g) \longrightarrow 3B_2O_2(g), \quad (2)$$

$$2B_2O_3(g) + 7C(s) \longrightarrow B_4C(s) + 6CO(g), \quad (3)$$

$$2B_2O_2(g) + 5C(s) \longrightarrow B_4C(s) + 4CO(g), \quad (4)$$

$$2B_2O_3(g) + 8CO(g) \longrightarrow B_4C(s) + 7CO_2(g), \quad (5)$$

$$2B_2O_2(g) + 6CO(g) \longrightarrow B_4C(s) + 5CO_2(g). \quad (6)$$

From the above chemical reactions, we can see that the generated B_2O_3, B_2O_2 and CO vapours were transferred to the energetically favoured sites of the substrate, and relative vapour–vapour reactions (Eqs.(5) and (6)) occur to form boron carbide nanobelts. Meanwhile, due to the fact that the Si wafer kept touching with the source powder materials during all the growth stages, and there were no Fe_3O_4 nanoparticles observed on the surface of the deposited Si wafer, the catalytic Fe_3O_4 nanoparticles may be transferred into the source powder materials after the reactions have been completed. In fact, we have observed that some 1D nanomaterials have been formed in the powder materials in the ceramic boat. To fully understand the growth mechanism of these rhomb-centred hexagonal boron carbide nanobelts, a systematic analysis of the growth kinetics is needed.

4. Conclusions

Single crystalline rhomb-centred hexagonal boron carbide nanobelts have been fabricated through a simple carbothermal reduction method with $B/B_2O_3/C/Fe$ powder as precursors at 1100°C. The growth of nanobelts is believed to be largely determined by growth kinetics. These nanobelts may find application in composites and nanothermal-electronics. Also, the nanobelt morphology may lead to product novel properties of boron carbide materials.

References

[1] Wood C and Emin D 1984 *Phys. Rev.* B **29** 4582

[2] Chen M W, McCauley J W and Hemker K J 2003 *Science* **299** 1563

[3] Sezer A O and Brand J I 2001 *Mater. Sci. Eng.* B **79** 191

[4] Lazzari R, Vast N, Besson J M, Baroni S and Dal Corso A 1999 *Phys. Rev. Lett.* **83** 3230

[5] Emin D and Aselage T L 2005 *J. Appl. Phys.* **97** 013529

[6] Xu F F and Bando Y 2004 *J. Phys. Chem.* B **108** 7651

[7] Ma R Z and Bando Y 2002 *Chem. Mater.* **14** 4403

[8] Ma R Z and Bando Y 2002 *Chem. Phys. Lett.* **364** 314

[9] Carlsson M, Garcia-Garcia F J and Johsson M 2002 *J. Cryst. Growth* **236** 466

[10] Johnsson M 2004 *Solid State Ionics* **172** 365

[11] Zhang D, McIlroy D N, Geng Y and Norton M G 1999 *J. Mater. Sci. Lett.* **18** 349

[12] McIlroy D N, Zhang D, Kranov Y and Norton M G 2001 *Appl. Phys. Lett.* **79** 1540

[13] Ma R Z, Bando Y, Sato T and Kurashima K 2001 *Chem. Phys. Lett.* **350** 434

[14] Dai H J, Wong E W, Lu Y Z, Fan S S and Lieber C M 1995 *Nature* **375** 769

[15] Han W, Bando Y, Kurashima K and Sato T 1999 *Chem. Phys. Lett.* **299** 368

[16] Han W, Kohler-Redlich P, Ernst F and Rohler M 1999 *Chem. Mater.* **11** 362

[17] Wei J Q, Jiang B, Li Y H, Xu C L, Wu D H and Wei B Q 2002 *J. Mater. Chem.* **12** 3121

[18] Pender M J and Sneddon L G 2000 *Chem. Mater.* **12** 280

[19] Welna D T, Bender J D, Wei X, Sneddon L G and Allcock H R 2005 *Adv. Mater.* **17** 859
[20] Zhang H Z, Wang R M, You L P, Yu Y, Chen H, Yu D P and Chen Y 2007 *New J. Phys.* **9** 13
[21] JCPDS-International Centre for Diffraction Data 2003 *PCPDFWIN* v.2.4
[22] He S T, Yao J N, Jiang P, Shi D X, Zhang H X, Xie S S, Pang S J and Gao H J 2001 *Langmuir* **17** 1571
[23] Shen C M, Su Y K, Yang H T, Yang T Z and Gao H J 2003 *Chem. Phys. Lett.* **373** 39
[24] Yang H T, Shen C M, Wang Y G, Su Y K, Yang T Z and Gao H J 2004 *Nanotechnology* **15** 70
[25] Yang H T, Shen C M, Su Y K, Yang T Z, Gao H J and Wang Y G 2003 *Appl. Phys. Lett.* **82** 4729
[26] Xiao C W, Yang H T, Shen C M, Li Z A, Zhang H R, Liu F, Yang T Z, Chen S T and Gao H J 2005 *Chin. Phys.* **14** 2269
[27] Wang X J, Tian J F, Yang T Z, Bao L H, Hui C, Liu F, Shen C M, Xu N S, Gu C Z and Gao H J 2007 *Adv. Mater.* **19** 4480
[28] Yang T Z, Shen C M, Li Z A, Zhang H R, Xiao C W, Chen S T, Xu Z C, Shi D X, Li J Q and Gao H J 2005 *J. Phys. Chem.* B **109** 23233
[29] Yang T X, Shen C M, Yang H T, Xiao C W, Xu Z C, Chen S T, Shi D X and Gao H J 2006 *Surf. Interface Anal.* **38** 1063
[30] Xia Y N, Yang P D, Sun Y G, Wu Y Y, Mayers B, Gates B, Yin Y D, Kim F and Yan Y Q 2003 *Adv. Mater.* **15** 353
[31] Wagner R S and Ellis W C 1965 *T. Metall. Soc. AIME* **233** 1053
[32] Zhang R Q, Lifshitz Y and Lee S T 2003 *Adv. Mater.* **15** 635